

Pseudopotential local-spin-density studies of neutral and charged Mg_n ($n \leq 7$) clusters

F. Reuse, S. N. Khanna,* V. de Coulon,[†] and J. Buttet

Institut de Physique Expérimentale, Ecole Polytechnique Fédérale de Lausanne, PHB-Ecublens, CH-1015 Lausanne, Switzerland

(Received 29 January 1990)

Electronic-structure calculations on neutral, anionic, cationic, and doubly ionized Mg_n ($n \leq 7$) clusters have been carried out to examine the effect of charging on the geometry and stability of clusters. Our studies employ Gaussian basis functions, treat exchange-correlation effects via the local-spin-density approximation, and use pseudopotentials to replace the cores. For neutral clusters we focus on the evolution of the nature of the electronic states as a function of size, and show that within an s - p -mixing criterion Mg_7 is not metallic. We find that the neutral clusters have compact equilibrium geometries, and that for $n > 4$ the ground-state geometries of the anionic and cationic clusters are obtained from the neutral clusters by small displacements of the atoms. Both cationic and anionic clusters are more stable than the corresponding neutral cluster, the mechanism by which the electron in anionic and the hole in cationic clusters enhance their stability is discussed. Our studies on doubly ionized clusters show that their geometries are dictated by the Coulomb repulsion between the holes and the electronic bonding forces. Mg_7^{2+} is the first doubly charged cluster whose equilibrium geometry is not a linear chain. All doubly charged cations are metastable, their dissociation barrier is calculated. We also present a complete study of the Born-Oppenheimer surfaces of neutral and ionized trimers, and discuss the importance of geometrical constraints on the ionization process.

I. INTRODUCTION

Small clusters constitute a new state of matter with electronic, magnetic, and chemical properties different from the atoms or solid. One of the features, which distinguishes them from condensed matter, is the near complete topological freedom, i.e., atoms may rearrange themselves in response to a perturbation. In particular, the addition or removal of a few electrons produces little change in bulk systems, however, such an addition or removal may have large effects in clusters and produce a change in geometry, electronic and magnetic behavior, or even lead to fragmentation.

The effect of charging on clusters is important to study in relation to several recent experiments that have given information on the cohesive energy and electronic properties of clusters: size-selected fragmentation experiments for both positively¹ and negatively² charged clusters, charge exchange between singly or doubly charged clusters and neutral species,³ negative-ion photoelectron spectroscopy,⁴ and Coulomb explosion⁵ of doubly charged clusters. A knowledge of the geometrical structure of the neutral and charged clusters is crucial to understand in detail the experimental results, at least for the small-size clusters ($n < \sim 10$). A theoretical input is thus needed since the experiments only give indirect information on the geometrical structure.

Over the past few years several *ab initio* theoretical studies on the geometrical and electronic properties of neutral metal clusters have been published,⁶ there are, however, fewer studies that have calculated the equilibrium geometry of charged metal clusters. The most detailed results have been obtained for alkali-metal clusters ($n \leq 9$), both positively^{7,8} and negatively charged,⁹ for Cu

cations and anions ($n \leq 4$) (Refs. 10 and 11) and Ag cations ($n \leq 4$) (Ref. 11), as well as for Si cationic¹² clusters ($n \leq 6$). The studies on the alkali- and noble-metal clusters reveal that the charging significantly changes the geometry, in particular for the anionic clusters that become linear chains for $n \leq 5$. There is also an increase^{7,9} in atomization energy from the neutral, to the anionic, and to the singly charged cationic cluster. For Si on the other hand, studies of singly ionized clusters indicate that there is no significant modification of the geometry.

We present here a comprehensive local-spin-density (LSD) study of the geometrical and electronic structure of anionic, neutral, singly, and doubly charged Mg_n ($n \leq 7$) clusters. In particular, we examine the importance of their geometry on several properties. A preliminary report of some of these results,¹³ as well as a previous study¹⁴ of Be clusters ($n \leq 5$), have already been published.

Bulk magnesium is a free-electron metal, it is thus at first tempting to describe the properties of Mg clusters in the framework of the jellium model,¹⁵ which has been so successful for alkali-metal clusters. However, in clusters of column-II elements there is an important evolution in the nature and strength of bonding as a function of size: it is known that their dimers are weakly bounded molecules,¹⁶ while the bulk phase is metallic. Recent experiments¹⁷ and theoretical papers¹⁸ have studied this evolution in mercury clusters, and a van der Waals to metallic transition has been suggested. However, no detailed *ab initio* analysis has yet been given. It is difficult to carry out calculations on Hg, since the presence of d electrons and relativistic effects have to be taken into account, and to our knowledge only *ab initio* studies on neutral¹⁹ and charged²⁰ dimers have been published.

It is easier to undertake calculations on Be clusters, which have a small number of electrons, and several *ab initio* theoretical studies on neutral Be molecules and clusters²¹ have been reported. The bonding in Be_n (*s-p* hybridization) converges quickly toward that of a metal, and from this point of view its behavior is very different compared with Hg. For Mg on the other hand our LSD results and configuration-interaction (CI) calculations²² show that the convergence toward the "bulk bonding" for neutral clusters is slower than in Be. Except for a study²³ of Mg_n clusters ($n \leq 5$) with a model potential, there is no systematic detailed investigations of charged clusters of column-II atoms.

One of the main results concerning the geometrical structure that appears from our studies, is that Mg_n clusters have a strong tendency to form compact structures, i.e., those which maximize the number of bonds. This is true for neutral, anionic, and singly ionized species, except for the $n = 3$ and 4 cations, which are linear chains. A similar result has been obtained for Be clusters¹⁴ and is probably also true for column-II elements in general.

Singly charged clusters are stable, multiply ionized clusters may, however, be unbound or metastable. Doubly ionized clusters have been the subject of numerous experimental and theoretical investigations,⁵ one of the key questions has been the minimum or critical cluster size n_c for which a doubly ionized cluster is observable. Recent experiments have reported very small critical numbers, it has for example been shown that Pb_3^{2+} ,²⁴ Au_2^{2+} ,³ Hg_5^{2+} ,²⁵ etc. are stable within the observation time of the measurement. This suggests the existence of a potential barrier preventing the clusters from dissociating. Theoretical studies on doubly charged transition metal²⁶ and Hg (Ref. 20) dimers show that only a detailed study implying short-range forces can account for the delicate balance between the cohesive and repulsive energies. Recently we reported studies¹⁴ on Be_n^{2+} ($n \leq 5$) clusters, where we found that the doubly ionized clusters are energetically unstable, however, their Born-Oppenheimer energy surface (BO surface) is characterized by deep minima. Under suitable experimental conditions, it should be possible to trap the clusters in these minima and, hence, observe them.

In this work we extend these studies to Mg_n^{2+} clusters and show that small Mg_n^{2+} ($n \leq 6$) are linear chains, while Mg_7^{2+} has a three-dimensional elongated structure and a small negative binding energy. We present complete results on the BO surfaces of the trimers and find that Mg_3^{2+} can only be created through sequential ionization. For $n \leq 6$ we calculate the dissociation energy and dissociation barrier of the lowest-energy fragmentation channels and discuss their relevance on the fragmentation process. The localization of the holes in the clusters is also examined, for the linear chains it is in agreement with the conventional picture that the holes are located as far apart as possible. The situation is different for other geometries and will be discussed.

This paper is organized as follows: In Sec. II we present our theoretical approach, Secs. III, IV, and V contain our results and a preliminary discussion on geometrical structure, binding energy, fragmentation

channels of, respectively, neutral, anionic, and cationic clusters. Section VI concentrates on doubly ionized clusters and Sec. VII contains a discussion mainly focused on the effect of charging on the geometrical structure and formation process of clusters. Finally, Sec. VIII gives a summary and discussion of our results.

II. DETAILS OF CALCULATIONS

All of our studies have been carried out within a linear combination of Gaussian functions, and core effects are incorporated through the use of nonlocal pseudopotentials.²⁷ The exchange and correlation contributions have been treated in the Hohenberg-Kohn-Sham local-density approximation, where we have employed the potential form proposed by Ceperley and Alder based on the numerical parametrization of Perdew and Zunger.²⁸

The basis set has been constructed via a nonlinear fit to the numerical *3s* and *3p* pseudo-wave-functions, obtained from a radial solution of the atomic Kohn-Sham equation. The basis functions were tested for their completeness in several ways. We calculated the one-electron eigenvalues and the total energy for the neutral and ionized Mg atom using our basis functions. These are compared with the corresponding values obtained by numerical integration of the Schrödinger equation in Table I. As one notices, the basis functions lead to energy values that differ by less than 0.05 eV from the numerical values. Our calculated first and second atomic ionization potentials are 7.63 and 15.06 eV, compared to the experimental values²⁹ of 7.64 and 15.03 eV, respectively. The basis set was also tested for its overcompleteness by carrying out an atomic calculation with an extra set of basis functions at various distances from the atomic site. The change in energy with the extra set moved from 5 to 10 a.u. was less than 3 meV. In Table II we give the basis functions employed in the present calculation.

We also studied the effect of including a *d* Gaussian

TABLE I. One electron energy levels and total energy (in hartrees) of neutral and ionized Mg atoms. Results using a numerical integration of the radial Kohn-Sham equation and a Gaussian basis set are given. The numbers in parentheses are the known experimental values for the ionization potentials.

Atom		Numerical procedure	Gaussian functions
Mg	<i>3p</i>	-0.052 98	-0.051 91
	<i>3s</i>	-0.175 74	-0.175 48
	total energy	-0.832 95	-0.833 82
Mg^+	<i>3p</i> ↑	-0.281 60	-0.279 57
	<i>3p</i> ↓	-0.210 22	-0.207 14
	<i>3s</i> ↑	-0.440 35	-0.440 52
	<i>3s</i> ↓	-0.346 06	-0.340 62
	total energy	-0.552 81	-0.553 36
	1st ionization potential	7.62 eV	7.63 eV (7.64 eV)
	2nd ionization potential	15.04 eV	15.06 eV (15.03 eV)

TABLE II. Exponents (a.u.) of the Gaussian basis set employed in this work. The 0.01* exponent was only used for Mg_2^- .

s	p
1.229 90	0.120 692
0.829 423	0.032 466
0.118 557	0.01*
0.043 026	

(exponent 0.14 a.u.) on the binding energy. We find that the increase in binding energy is about 10%, therefore the correction due to the inclusion of d functions is relatively weak. Furthermore, it is well known^{16,30} that for small clusters of column-II elements the LSD approximation overestimates the binding energy (see Sec. III). Given the numerical complexity introduced by the inclusion of d functions and the approximations inherent in LSD, we have neglected to insert them in our basis set.

For anionic clusters the extra electron may present a diffuse character and require additional basis functions for a proper description. For Mg_2^- we found it necessary to augment the basis set by the extra Gaussian given in Table II. For Mg_3^- and bigger anionic clusters, the extra diffuse Gaussian was not necessary and was not used. The effect of the pseudopotential approximation has been tested for Mg_2 by comparing the results of an all electron calculation (11s, 7p per atom) with the pseudopotential results. We have found within, respectively, 2% and 0.1 a.u. the same binding energy and equilibrium distance.

The electronic-structure calculations were carried out using Gaussian functions to expand the cluster orbitals $|\psi_{\sigma\nu}\rangle$, $\sigma = \text{up or down}$ and $\nu = 1, 2, \dots$,

$$|\psi_{\sigma\nu}\rangle = \sum_i c_{\sigma\nu}^i |g_i\rangle,$$

where $|g_i\rangle$ are Gaussian functions and $c_{\sigma\nu}^i$ are coefficients determined from the Kohn-Sham equation³¹

$$\left(-\frac{1}{2}\Delta + V_{\text{ion}} + V_H + V_{\text{xc}}^\sigma\right) |\psi_{\sigma\nu}\rangle = \epsilon_{\sigma\nu} |\psi_{\sigma\nu}\rangle.$$

Here V_{ion} is the ionic pseudopotential, V_H is the Hartree potential and V_{xc}^σ the exchange-correlation potential.²⁸

The total energy is calculated via the expression

$$E = \sum_{\sigma,\nu} \langle \psi_{\sigma\nu} | \left(-\frac{1}{2}\Delta + V_{\text{ion}}\right) | \psi_{\sigma\nu} \rangle + \frac{1}{2} \int \int \frac{\rho(\mathbf{r})\rho(\mathbf{r}')}{|\mathbf{r}-\mathbf{r}'|} d^3\mathbf{r} d^3\mathbf{r}' + \int \epsilon_{\text{xc}}(\mathbf{r})\rho(\mathbf{r}) d^3\mathbf{r} + \sum_{1 \leq i < j \leq N} \frac{Z_i Z_j}{|\mathbf{R}_i - \mathbf{R}_j|},$$

where

$$\rho_\sigma(\mathbf{r}) = \sum_\nu |\psi_{\sigma\nu}(\mathbf{r})|^2 \text{ and } \rho(\mathbf{r}) = \sum_\sigma \rho_\sigma(\mathbf{r})$$

denotes the electronic density at \mathbf{r} , $\epsilon_{\text{xc}}(\mathbf{r})$ the exchange-correlation energy per electron, Z_i and \mathbf{R}_i

($i = 1, 2, \dots, N$), respectively, denote the charge and the position of ions.

The ground-state geometries were obtained by systematic exploration of subsets of the Born-Oppenheimer (BO) surface, characterized by symmetry constraints. We restricted, for example, the search to clusters with a plane and/or an axis of symmetry. These subsets were chosen taking into account symmetry arguments, the possibility of Jahn-Teller distortions, and the ground-state geometry of the previous cluster size. For neutral clusters we have also searched for geometrical structures derived from a two-, three-, and four-body effective potential calculation.³² In order to verify that the ground-state geometry corresponds to a minimum of the BO surface, we have randomly generated several configurations situated around the minimum.

III. NEUTRAL Mg_n CLUSTERS

A. Geometrical structure and bonding

In Fig. 1 we show the ground-state configurations of neutral Mg_n ($n \leq 7$) clusters. We also give their atomization energies and an angular decomposition of the molecular charge density using a Mulliken population analysis. As seen from Fig. 1, the ground-state geometries of Mg_n clusters are compact structures, Mg_4 is a tetrahedron, Mg_5 a triangular bipyramid, Mg_6 a bipyramid with rec-

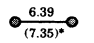
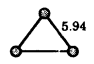
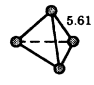
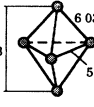
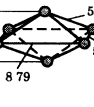


Cluster size	Equilibrium geometry (a.u.)	Atomization energies (eV)			Valence electrons Mulliken popul./e ⁻	
		AE	AE/atom	AE/bond	s	p
2		0.22	0.11	0.22	0.94	0.06
3		0.78	0.26	0.26	0.87	0.13
4		2.00	0.50	0.33	0.80	0.20
5		2.50	0.50	0.28	0.83	0.17
6		3.15	0.53	0.29	0.83	0.17
7		4.23	0.60	0.26	0.81	0.19
bulk hcp		1.52*	0.25*		0.39*	0.56*

FIG. 1. Equilibrium geometry, atomization energy (AE), and valence electron Mulliken population of neutral Mg clusters. Distances are given in atomic units and energies in eV. The numbers marked with an asterisk are the known experimental values. The bulk Mulliken population is taken from Ref. 40.

tangular basis, and Mg_7 a pentagonal bipyramid. They all correspond to singlet states. We have summarized all results concerning the geometries of neutral and charged clusters in Fig. 13 at the end of the paper. In this figure we also report several of the isomer geometries which have been calculated. We find in particular for $n = 6$ that the square bipyramid isomer with a singlet spin corresponds to the minimum energy in the family of the bipyramids with a rhombus basis. The square bipyramid leads, however, through a Jahn-Teller distortion to the bipyramid with rectangular basis. Notice that the $n = 5$ and $n = 6$ Mg structures can be considered as substructures of the bulk hcp geometry. In Fig. 1 the atoms of the bulk geometry corresponding to the $n = 6$ cluster are indicated with dots, the corresponding distances for the hexamer and the bulk substructure are, respectively, equal to 5.30, 5.82, 5.90, 8.79 and 6.03, 6.05, 6.05, 8.57.

The geometries obtained for the neutral clusters ($n \leq 5$) are similar to those reported in the literature ($n \leq 4$) for Mg clusters²² and to those geometries found for beryllium using both CI (Ref. 21) and LSD methods.¹⁴ The geometries obtained for Mg_6 and Mg_7 , however, differ from those of Be_6 and Be_7 , which have been found by CI (Ref. 21) to be, respectively, an octahedron with a quintet spin state and a pentagonal bipyramid with a quintet spin state. We have verified for Mg_6 that the square bipyramids with a triplet and a quintet state are higher in energy by more than 1 eV than the square bipyramid with rectangular base. In the heptamer case we have verified too that the pentagonal bipyramids with spins $S = 1$ and 2 are higher in energy than the singlet ground state.

One notices from Fig. 1 that the atomization energy per atom increases monotonically with cluster size. This is related to the increasing s - p mixing. In the metal, which has a higher atomization energy per atom than in Mg_7 , the s - p mixing is also larger. This indicates that the promotion of electrons from $3s$ to $3p$ states is an important mechanism responsible for the bonding in both the clusters and the metal. Such a remark had already been made on the basis of CI calculations²² of alkaline earths X_4 and X_{13} . It was also pointed out¹⁶ that the larger binding energy of Be clusters is mainly due to the larger interatomic s - p overlap and therefore to the larger s - p mixing in Be than in Mg. We have found the same behavior in our Be LSD calculations.¹⁴

It is interesting to note that the Mg_n clusters' geometries differ significantly from those of sodium clusters,^{7,8} which have only one $3s$ valence electron per atom, and from those of Al clusters,³³ which have an additional $3p$ electron per atom. In Mg_n the three-dimensional structures already appear at $n = 4$, whereas in Na_n clusters one has to wait till $n = 7$ to see true ground-state three-dimensional species. In Al ($n \leq 6$) the tendency is towards fcc substructures, but not necessarily to close-packed geometries.

In the case of Na clusters, it has been shown⁷ that the planar behavior can be understood by taking into account the delocalized behavior of the $3s$ -derived molecular orbitals and the successive filling of orbitals of s , p_x , p_y , and p_z symmetry. Notice also that Jahn-Teller distortions for compact structures of alkali-metal clusters already ap-

pear at $n = 3$, whereas they only appear at $n = 6$ for compact structures of group-II elements. In the case of Al clusters, the cohesion results from the delocalized $3p$ -derived orbitals. However, the interaction between the $3s$ - and $3p$ -derived orbitals destabilizes the cluster,³³ there is thus a tendency to form high-symmetry clusters in which a maximum number of bonding $3p$ orbitals are orthogonal by symmetry to the $3s$ orbitals. In the case of Mg the $3p$ -derived orbitals are not occupied, and contrary to the case of Al clusters the $3s$ - $3p$ mixing has a strong stabilizing effect.

It is important to point out that our calculation predicts a binding energy of 0.22 eV for Mg_2 compared to the experimental values of 0.052 eV. This is similar to Be_2 , where the LSD calculation¹⁴ leads to a binding energy of 0.36 eV, compared to the experimental value of 0.11 eV. The picture that emerges from CI calculations²² is that for dimers of group-II elements the energy gained by forming a single bond is not sufficient to overcome the promotion energy, and thus only a weak van der Waals bond is formed for Mg_2 and probably also for Mg_3 . Only a detailed and thorough treatment of electron correlation effects³⁴ can reproduce the experimental value of the binding energy for the dimer. The question of the adequacy of LSD to treat dimers of group-II elements has been addressed by Williams and von Barth³⁵ on the basis of the LSD calculations of Jones.¹⁶ The conclusion drawn from these analyses and our results is that the basic physical picture and trends are correctly reproduced in a LSD formalism, although for small clusters the binding energy of the neutrals is too large. Furthermore, it is expected that the LSD results will be better the larger the size of the cluster, e.g., a LSD calculation of bulk Be (Ref. 36) reproduces the bulk cohesive energy within a few percent of the experimental value. We also expect LSD to provide a good description of positively charged clusters that are strongly bonded. For example a recent CI calculation reports a binding energy of 2.0 eV for Be_2^+ (Ref. 37), while the LSD value is 2.2 eV.¹⁴

B. The van der Waals to metal transition

The elements of column II, as already mentioned in the Introduction, raise the interesting question of the van der Waals to metal transition. Theoretical analyses,³⁸ made in relation with the metal-to-nonmetal phase transition in liquid mercury, have shown that when the coordination number increases there is a gradual decrease of the gap between the s and p bands. Metallic behavior appears when there is overlap and mixing of the s and p bands. The same situation is true for clusters when the size, and therefore the mean coordination number increases, as has been shown in tight-binding calculation.¹⁸ On the experimental side, recent photoelectron experiments on Hg clusters³⁹ have shown that when the cluster size is increasing there is a gradual "band broadening" and there are indications of the mixing of the " s and p bands." This suggests that for clusters of group-II elements the mixing of the s - and p -derived orbitals can be taken as a simple criteria of the onset of metallic behavior. It is interesting to examine this for Mg clusters.

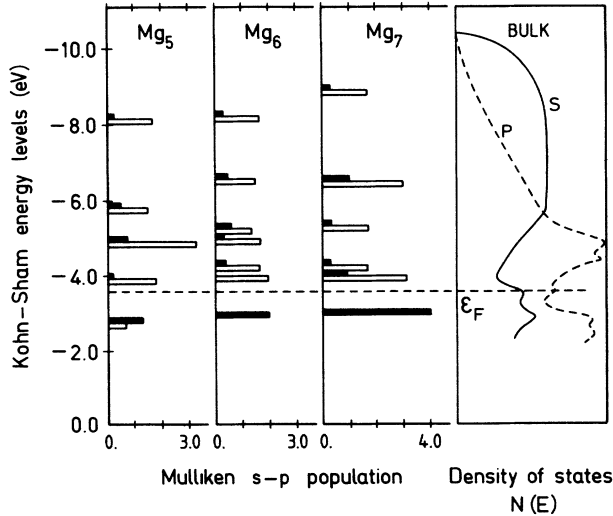


FIG. 2. Mulliken population analysis of the Kohn-Sham energy levels of Mg_n ($n = 5, 6,$ and 7). The white bars correspond to the s population and the black bars to the p population calculated for each Kohn-Sham orbital. The bulk s and p density of states are taken from Ref. 40.

Figure 2 shows the position of the Kohn-Sham energy levels for Mg_5 , Mg_6 , and Mg_7 and for each level the decomposition into s and p components. On the same graph we also show the bulk density of states⁴⁰ decomposed into its s and p parts. There is a clear indication of band broadening when the size increases, however, the mixing of the s and p angular components is much smaller in Mg_7 than in the bulk case. From this point of view, Mg_7 has not yet reached the metallic state. Using the s - p mixing criterion a similar analysis done for Be_5 indicates that Be_5 is much closer to a metal than Mg_7 . This contrasting behavior is related to the stronger overlap of the s and p atomic wave functions in Be than in Mg, as mentioned earlier. In Be_5 it appears that the number of nearest neighbors is already large enough, so that the nature of the bonds in the cluster is similar to that in the solid. For example the p part of the valence states for Be_5 and the bulk are, respectively, equal to 0.48 and 0.67. For Mg, which has a weaker bond, we expect that the increasing number of nearest neighbors, when the size of the cluster increases beyond seven atoms, has still a significant effect on the nature of the bond formed. A similar situation probably also exists for mercury clusters.

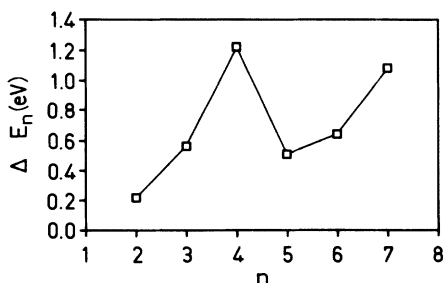


FIG. 3. Sublimation energy $\Delta E_n = E_{n-1} + E_1 - E_n$ as a function of n . The energies are given in eV.

TABLE III. Lowest-energy fragmentation channels of neutral Mg_n clusters. The energies are given in eV.

$Mg_{n+m} \rightarrow Mg_n + Mg_m$	$E_n + E_m - E_{n+m}$ (eV)
$Mg_2 \rightarrow Mg + Mg$	0.21
$Mg_3 \rightarrow Mg_2 + Mg$	0.56
$Mg_4 \rightarrow Mg_3 + Mg$	1.22
$\rightarrow Mg_2 + Mg_2$	1.56
$Mg_5 \rightarrow Mg_4 + Mg$	0.53
$\rightarrow Mg_3 + Mg_2$	1.52
$Mg_6 \rightarrow Mg_5 + Mg$	0.59
$\rightarrow Mg_4 + Mg_2$	0.90
$Mg_7 \rightarrow Mg_6 + Mg$	1.12
$\rightarrow Mg_4 + Mg_3$	1.46

C. Fragmentation channels

Important information about stability is obtained through studies of fragmentation channels. Starting from a cluster size $n + m$, we have calculated the energy difference ΔE required to break a cluster into sizes n and m , where

$$\Delta E = (E_n + E_m) - E_{n+m}.$$

Here E_{n+m} , E_n , and E_m are the total energies of clusters having $n + m$, m , and n atoms. In Table III, we present the lowest and the next higher dissociation channels for neutral Mg_n clusters. All Mg_n clusters up to $n = 7$ fragment preferentially by evaporating a single Mg atom. Mg_4 appears to be particularly stable against fragmentation, this is clearly seen in Fig. 3 where we plot the sublimation energy $\Delta E_n = E_{n-1} + E_1 - E_n$ as a function of n .

IV. ANIONIC Mg_n^- ($n \leq 7$) CLUSTERS

The study of anionic clusters raises several questions in the framework of the local-spin-density approximation, since the form of the LSD exchange-correlation potential is incorrect at large distances.⁴¹ In particular it has been found for anionic atoms, and we have verified it in the case of Mg_n^- clusters, that the one-electron eigenvalue of the extra electron is slightly positive. However, for atoms it has been shown⁴² that, if the extra electron is artificially confined to a region near the atom through localized bases, the difference in the LSD total energy between negatively charged and neutral atoms is a measure of the electron affinity. The same is true for molecules and clusters. For example a recent CI calculation of Be_2^- (Ref. 37) finds an adiabatic electron affinity equal to 0.56 eV, while the value that we have found in a LSD Be pseudopotential calculation⁴³ is equal to 0.61 eV. As we show later, this is further borne out by a comparison with measured electron affinities.

A. Geometrical structure and bonding

In Fig. 4 we show the geometries of anionic Mg_n^- ($n \leq 7$) clusters. We also give the atomization energy per atom, the symmetry, and an angular decomposition of

the extra electron orbital. A comparison between Figs. 1 and 4 shows that for $n \leq 6$ the anionic clusters have the same equilibrium geometries as the neutral clusters. For $n = 7$ the minimum energy geometry is a distorted pentagonal bipyramid. The distortion has been obtained in assuming that the plane passing through the five atoms of the base remains a symmetry plane, and that there is an additional symmetry plane passing through one of the basis atom and the two summit atoms. This procedure, however, still leaves six free parameters, and the equilibrium geometry has been found by minimizing the energy with respect to all six parameters. Figure 4 also indicates that the anionic clusters are more stable than the neutral clusters; they have an extra atomization energy of about 0.2 eV/atom over the neutral clusters.

To investigate the behavior of negatively charged clusters in more detail, in Fig. 4 we give a pictorial representation of the symmetry of the extra electron orbital. For Mg_2^- we find that the outer electron occupies a π bonding orbital, formed from p atomic orbitals perpendicular to the molecular axis. Since there was a controversy on the nature of this extra electron orbital for Be_2^- , we have extensively investigated the charge localization in Mg_2^- by including additional diffuse p functions oriented along the axis of the molecule. The extra electron orbital, how-

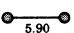
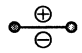



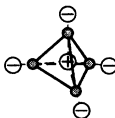
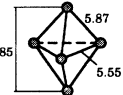
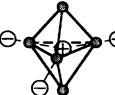
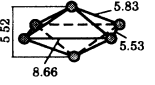
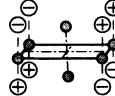
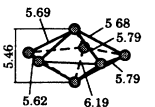
Cluster size	Equilibrium geometry (a.u.)	AE/atom	Symmetry extra orbital	Extra electron Mulliken popul.	
				s	p
2		0.29		0.00	1.00
3		0.57		0.00	1.00
4		0.74		0.36	0.64
5		0.74		0.37	0.63
6		0.76		0.00	1.00
7		0.81		0.00	1.00

FIG. 4. Equilibrium geometry, atomization energy per atom (AE/atom), symmetry of the extra electron orbital, and extra orbital Mulliken population analysis of singly negatively charged Mg clusters. The atomization energy is defined as the difference between the energy of n separated atoms and the energy of Mg_n^- . Distances are given in atomic units and energies in eV.

ever, always occupied a π orbital, which is represented in Fig. 5(a). This is in agreement with the latest calculation for Be_2^- (Refs. 37 and 44). For the other anionic clusters ($n \leq 6$) the extra electron occupies a nondegenerate molecular orbital, invariant under the symmetry group of the cluster. As an example, we represent in Fig. 5(b) the case of Mg_4^- , where the extra electron orbital is formed predominantly of p atomic functions directed toward the center of the tetrahedron. Its symmetry is in agreement with the results of a previous calculation⁴⁵ done on Be_4^- , and it clearly corresponds to a bonding orbital. The case of $n = 6$ is interesting since the orbital is symmetric with respect to a plane perpendicular to the rectangular base and antisymmetric with respect to the other perpendicular plane. It is thus bonding in one direction and antibonding in the other. This behavior explains the rectangular shape of the basal plane of the hexamer geometry.

An analysis of the one-electron levels indicates that for $n \leq 6$ there is no Jahn-Teller distortion induced by adding an electron to a neutral cluster. This is why the equilibrium geometries of anionic and neutral clusters have the

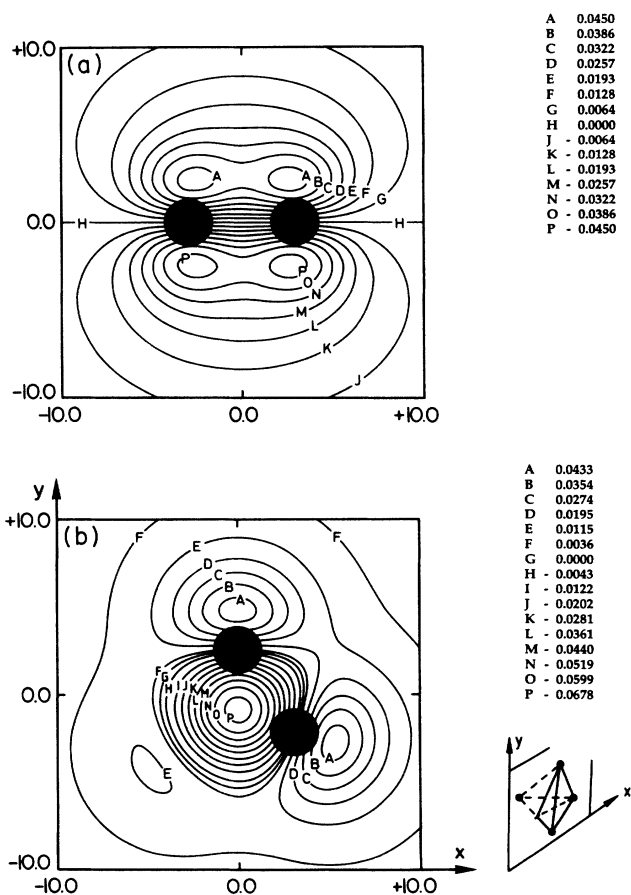


FIG. 5. Contour plot of the extra electron molecular orbital in singly negatively charged Mg clusters; (a) is given for a Mg_2^- cluster and (b) for a Mg_4^- cluster, the chosen plane is indicated in the figure. The length scale is given in atomic units, the amplitude of the wave function (table on the right-hand side) is given in units of electrons per (cubic atomic unit)^{1/2}. The shaded areas show the extension of the atomic cores.

TABLE IV. Lowest-energy fragmentation and electron detachment channels of anionic Mg clusters. DE is the dissociation energy; Vert. EA the vertical electron affinity; Expt. EA corresponds to experimental values of the EA obtained by photoelectron detachment spectroscopy (Ref. 47). The underlined numbers give the calculated adiabatic EA.

Dissociation channels	DE (eV)	Vert. EA (eV)	Expt. EA (eV)
$\text{Mg}_2^- \rightarrow \text{Mg}_2 + e^-$	<u>0.38</u>	0.39	
$\text{Mg}_3^- \rightarrow \text{Mg}_3 + e^-$	<u>0.90</u>	0.93	0.9 ± 0.1
$\rightarrow \text{Mg}_2^- + \text{Mg}$	1.08		
$\text{Mg}_4^- \rightarrow \text{Mg}_4 + e^-$	<u>0.99</u>	1.00	1.15 ± 0.1
$\rightarrow \text{Mg}_3^- + \text{Mg}$	1.29		
$\text{Mg}_5^- \rightarrow \text{Mg}_4^- + \text{Mg}$	0.63		
$\rightarrow \text{Mg}_5 + e^-$	<u>1.09</u>	1.14	1.2 ± 0.1
$\text{Mg}_6^- \rightarrow \text{Mg}_5^- + \text{Mg}$	0.90		
$\rightarrow \text{Mg}_4^- + \text{Mg}_2$	1.32		
$\rightarrow \text{Mg}_6 + e^-$	<u>1.40</u>	1.46	1.3 ± 0.2
$\text{Mg}_7^- \rightarrow \text{Mg}_6^- + \text{Mg}$	1.17		
$\rightarrow \text{Mg}_7 + e^-$	<u>1.46</u>	1.52	

same group symmetry. This is not the case for $n=7$, where the first nonoccupied orbital in the neutral cluster is twofold orbitally degenerate, but since the cluster is large, the Jahn-Teller distortion is small. Note in contrast that in one-valence electron atoms, such as Li (Ref. 9) and Cu (Ref. 10) the addition of an extra electron produces changes in the geometry of the clusters, which become linear chains ($n \leq 5$). For Mg_3^- and Mg_4^- we find the linear geometries to be, respectively, 0.4 and 1.1 eV higher in energy than the equilibrium geometries.

B. Photofragmentation and photodetachment

The theoretical study of the dissociation channels of anionic clusters is an interesting problem, since it gives information on the competition between photofragmentation and photodetachment, which has been observed in recent experiments.⁴⁶ The results that we have obtained are summarized in Table IV. It is seen that small anionic Mg_n^- ($n \leq 4$) clusters require less energy for photodetachment than for photofragmentation, while for larger Mg_n^- ($n > 4$) clusters the situation is the opposite. These results are related to the branching ratio of photodetachment and photofragmentation channels. In Table IV we also compare the vertical electron affinities obtained in this work with recent experimental values obtained by photodetachment spectroscopy on jet-cooled clusters.⁴⁷ It is gratifying to note that the agreement is very good. Notice also that the vertical and adiabatic electron affinities are similar, since there is little change in geometry from the anionic to the neutral cluster.

V. CATIONIC Mg_n^+ CLUSTERS

We now describe the properties of ionized clusters. The geometries and binding energies for the cationic clusters are given in Fig. 6. Except in the case of very small clusters ($n=3$ and 4), whose equilibrium geometry are linear chains, the ground state geometries of the singly

ionized clusters are not very different from those obtained for the parent neutral clusters. For the tetramer (see Fig. 13) the planar rhombus and the triangular pyramid are only, respectively, 0.07 and 0.15 eV higher in energy than the linear chain. It is thus difficult to decide which isomer corresponds to the true ground state. For Mg_5^{2+} the

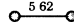
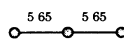
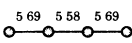
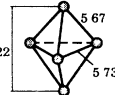
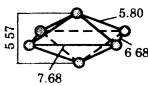
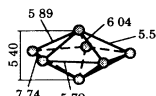
Cluster size	Equilibrium geometry (a.u.)	Atomization energies (eV)	
		AE	AE/atom
2		1.52	0.76
3		2.54	0.85
4		3.33	0.83
5		4.63	0.93
6		5.05	0.84
7		6.30	0.90

FIG. 6. Equilibrium geometry and atomization energy (AE) of singly ionized clusters. The atomization energy is defined as $(n-1)E + E^+ - E_n^+$, where E and E^+ are the energies of, respectively, neutral and singly ionized atoms. Distances are given in atomic units, and energies in eV.

TABLE V. Lowest-energy fragmentation channels of cationic Mg_n^+ clusters. The energies are given in eV.

$Mg_{n+m}^+ \rightarrow Mg_n^+ + Mg_m$	$E_n^+ + E_m - E_{n+m}^+$
$Mg_2^+ \rightarrow Mg^+ + Mg$	1.53
$Mg_3^+ \rightarrow Mg_2^+ + Mg$	1.03
$Mg_3^+ \rightarrow Mg^+ + Mg_2$	2.34
$Mg_4^+ \rightarrow Mg_3^+ + Mg$	0.77
$Mg_4^+ \rightarrow Mg_2^+ + Mg_2$	1.59
$Mg_5^+ \rightarrow Mg_4^+ + Mg$	1.30
$Mg_5^+ \rightarrow Mg_3^+ + Mg_2$	1.87
$Mg_6^+ \rightarrow Mg_5^+ + Mg$	0.39
$Mg_6^+ \rightarrow Mg_4^+ + Mg_2$	1.48
$Mg_7^+ \rightarrow Mg_6^+ + Mg$	1.26
$Mg_7^+ \rightarrow Mg_5^+ + Mg_2$	1.43

square bipyramid and the linear chain are, respectively, 0.31 and 0.64 eV higher in energy than the ground-state triangular bipyramid. Notice also that the seven atom cationic cluster is a Jahn-Teller distortion of the regular pentagonal bipyramid obtained for the corresponding neutral cluster.

Figure 6 indicates that the cationic clusters are more stable than the parent neutral and anionic clusters. This can be understood in a simple model, since the removed electron is taken from an antibonding orbital. In order to investigate this more carefully we have compared the electronic density of the missing orbital with the difference in electronic density between a singly charged cluster and a neutral cluster with the same geometrical structure as the corresponding cationic cluster. This analysis shows that there is little charge rearrangement when a single electron is taken out of a neutral cluster, contrary to the situation of the doubly charged clusters. This is in agreement with the qualitative picture of frozen orbitals, which is implicit in a simple description of the increased bonding for singly charged clusters of column II.

Several experimental studies of the fragmentation of cationic clusters have been reported for alkali-, semiconducting-, and transition-metal clusters. Given a cationic cluster Mg_{n+m}^+ fragmenting into sizes n and m , the basic issue is to know which fragment is left with the missing electron and what are the branching ratios of the different fragmentation channels. In Table V we show the lowest dissociation channels as well as the dissociation energies of cationic clusters. The lowest dissociation channel always corresponds to the evaporation of a neutral Mg atom, while the remaining fragment carries the missing electron. This is in agreement with most experimental data for small clusters. It is interesting to notice that, in contrast with Si clusters,¹² where Si_4^+ and Si_6^+ are particularly stable, Mg_4^+ and Mg_6^+ have the lowest fragmentation energies.

VI. COULOMB EXPLOSION OF Mg_n^{2+}

As mentioned in the Introduction there is considerable experimental and theoretical interest in the fragmentation of doubly ionized clusters. One of the quantities of interest is the minimum cluster size n_c , for which a dou-

bly charged cluster is experimentally observable. Another question of experimental interest is the determination of the preferred dissociation channels. We shall show that for metastable systems they are not only related to the final-state energies of the dissociation products, but also to the height of the dissociation barrier.

A. Geometrical structure

In Fig. 7 we show the lowest-energy configurations of the doubly ionized Mg_n ($n \leq 7$) clusters, their atomization energies, and for the lowest-energy fragmentation channels the dissociation energies and the height of the potential barrier. We also give in Fig. 13 the geometrical structure of most of the low-energy isomers that we have calculated. All doubly ionized clusters up to $n=6$ are linear chains, there are, however, two- or three-dimensional isomers with a large number of bonds not much higher in energy. For $n=7$ the minimum energy configuration corresponds to a pentagonal bipyramid with one atom added on each summit. The linear chain is only 0.08 eV higher in energy, the next isomer is a cen-

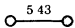
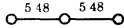
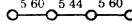
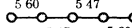
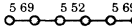
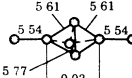
Cluster size	Atomization energies (eV)	Equilibrium geometry	Dissoc. channel	Dissoc. energy (eV)	Barrier (eV)
2	-1.27		$Mg^+ + Mg^+$	-2.54	0.48
			$Mg^{++} + Mg$	4.88	
3	0.07		$Mg_2^+ + Mg^+$	-1.30	0.77
			$Mg^+ + Mg^+ + Mg$	0.22	
4	0.53		$Mg_2^+ + Mg_2^+$	-0.92	0.90
			$Mg_3^+ + Mg^+$	-0.41	0.82
			$Mg_2^+ + Mg^+ + Mg$	0.61	
5	0.72		$Mg_3^+ + Mg_2^+$	-0.48	0.98
			$Mg_4^+ + Mg^+$	0.25	
6	0.80		$Mg_3^+ + Mg_3^+$	-0.29	1.03
			$Mg_4^+ + Mg_2^+$	-0.05	1.03
			$Mg_5^+ + Mg^+$	0.15	
7	0.84		$Mg_5^+ + Mg_2^+$	-0.27	
			$Mg_4^+ + Mg_3^+$	0.02	

FIG. 7. Equilibrium geometry, atomization energy, and dissociation channels of doubly ionized clusters. The atomization energy is defined as $(n-2)E + 2E^+ - E_n^{2+}$. The dissociation energy measures the difference in energy between the fragments and the parent cluster, a minus sign indicates that Mg_n^{2+} is metastable with respect to the corresponding fragments. The barrier height has been calculated in assuming that the interatomic distances of the separated fragments correspond to the equilibrium geometry of isolated fragments. Only linear configurations have been considered. Distances are given in atomic units, and energies in eV.

tered hexagon, which corresponds to the minimum-energy configuration of an hexagonal pyramid. As in the case of Be clusters¹⁴ the geometrical structure of Mg_n^{2+} is a delicate balance between the effect of the Coulomb repulsion, which tends to give elongated structures in order to minimize the repulsive energy of the holes, and the attractive bonding energy that increases with the number of bonds. In this respect the $n = 7$ structure is particularly interesting, since it realizes a compromise between these two competing effects. When the size increases, the cohesive energy of the bonds will be the dominant factor and the equilibrium configurations of the doubly ionized clusters will tend toward compact three-dimensional structures, similar to those obtained for the neutral and singly ionized clusters.

B. Dissociation of linear chains

From Fig. 7 we notice that all doubly ionized clusters are energetically unstable toward fragmentation. However, a detailed study of the BO surface indicates that the energy hypersurface is marked by deep minima. If the cluster could be prepared to lie in this minimum, it would be protected from fragmentation by barriers and thus could be observable.

The situation for Mg_2 is summarized in Fig. 8, where we have represented the energy as a function of the interatomic spacing for the neutral, singly and doubly charged dimers. It is clear from this graph that Mg_2 and

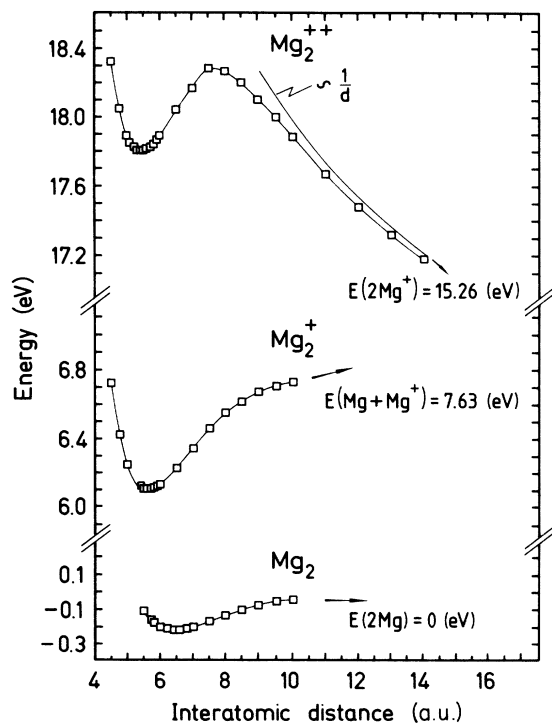


FIG. 8. Energy as a function of the interatomic distance of neutral, singly, and doubly ionized Mg dimers. The zero of energy corresponds to the energy of two neutral atoms. The $1/d$ curve is the Coulomb repulsion term, calculated in assuming that there is one electronic charge on each nucleus. Distances are given in atomic units and energies in eV.

Mg_2^+ are stable toward dissociation, while Mg_2^{2+} is metastable. The height of the dissociation barrier is equal to 0.48 eV, and a simple WKB approximation shows that at low temperature a doubly charged dimer can exist in the potential well for long times compared to the typical 10- μ s observation time. Some care has to be taken in looking at dissociation curves, since at large distances the electrons on two separated fragments are uncorrelated. For symmetric molecules it is important that the wave function has the flexibility of symmetry breaking, in this respect Mg_2^{2+} is very similar to the H_2 molecule.⁴⁸ However, similar precautions have also to be taken when the cluster dissociates into nonequivalent fragments, for example the dissociation of Mg_4^{2+} into Mg_3^+ and Mg^+ . We have also reported the Coulomb repulsion term in Fig. 8, it was calculated in assuming that there is a point charge on each atom. This graph clearly shows that when the interatomic distance is greater than approximately 10 a.u. the Coulomb term is the only remaining interaction. The picture that we can draw from these curves is simple. When two singly ionized atoms are approached from infinity they first interact through their Coulomb repulsion term. When their separation is of the order of 10-a.u., short-range interactions set in, a bond is formed and the energy decreases toward a metastable minimum. Such a picture is basically valid for the dissociation of all doubly charged clusters of group-II elements, there are, however, second-order effects related to the polarizability of the clusters, which should be added to the Coulomb repulsion term.

In the case of the doubly ionized trimer we have done a complete study of the BO surface in varying the two interatomic distances and the apex angle, and more than 250 configurations have been calculated. We give in Fig.

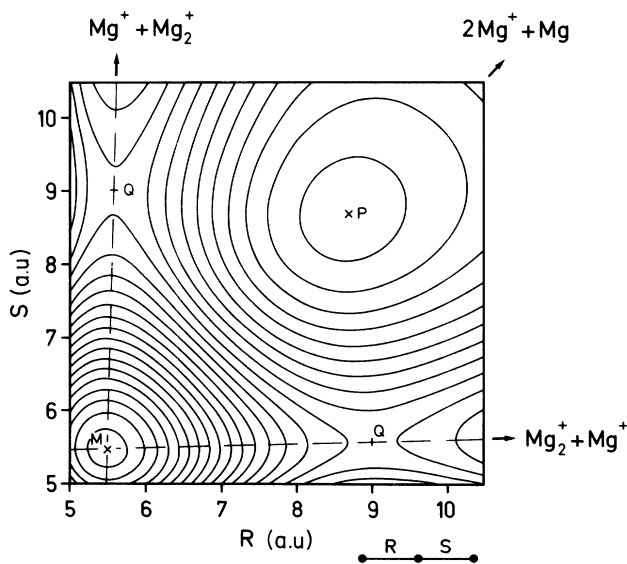


FIG. 9. Born-Oppenheimer surface of linear Mg_3^{2+} . The separation in energy between each constant energy curve is equal to 0.045 eV. M corresponds to the equilibrium geometry, Q and P to the geometrical configuration associated with the maximum height of the potential barrier for dissociation into, respectively, $Mg_2^+ + Mg^+$ and $2Mg^+ + Mg$. The dashed line is the lowest-energy dissociation path.

9 a two-dimensional contour plot of the BO surface for a linear chain. This graph clearly shows the dissociation path of Mg_3^{2+} into Mg_2^+ and Mg^+ , the potential barrier maximum at point Q corresponding to a barrier height of 0.77 eV, as well as the slight expansion of the interatomic distance from the value calculated for the doubly charged trimer to that of the single ionized dimer. The dissociation into two singly ionized and a neutral atom is also shown. The corresponding dissociation path is a straight line passing through point P , which corresponds to the maximum of the barrier height.

As a final example, in Fig. 10 we give the energy of the dissociating Mg_4^{2+} as a function of the distance of two singly ionized fragments. The zero of energy corresponds to the energy of two ionized dimers. Figure 10(a) corresponds to the fission process $\text{Mg}_4^{2+} \rightleftharpoons \text{Mg}_2^+ + \text{Mg}_2^+$ and Fig. 10(b) to the evaporation process $\text{Mg}_4^{2+} \rightleftharpoons \text{Mg}_3^+ + \text{Mg}^+$. One notices (see Fig. 7) that the fission process is lower in energy than the evaporative one, however, the potential barrier for fragmentation into two equal mass fragments is higher than for the evaporation of Mg^+ . This indicates that evaporation will be favored over fission, even though the final energy is higher. This result shows that for metastable systems the standard explanation of the branching ratio for the fragmentation processes, which asserts that the channels with the largest energy gain are favored, is questionable.

We have not done a study of all dissociation processes for Mg_5^{2+} and Mg_6^{2+} , which are also linear chains. It is, however, interesting to notice (see Fig. 7) that the barrier height for dissociation increases as a function of cluster size, and tends to level at a value of about 1 eV. This lev-

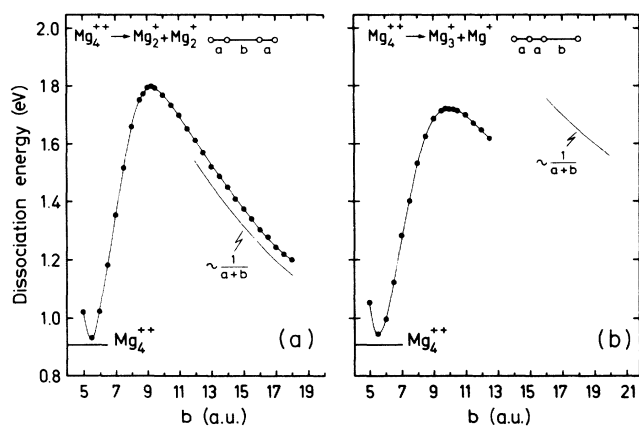


FIG. 10. Energy of Mg_4^{2+} as a function of the distance between two separated singly ionized fragments; (a) corresponds to the fission process $\text{Mg}_4^{2+} \rightleftharpoons \text{Mg}_2^+ + \text{Mg}_2^+$ and (b) to the evaporation process $\text{Mg}_4^{2+} \rightleftharpoons \text{Mg}_3^+ + \text{Mg}^+$. The energy has been calculated in assuming that the interatomic distances of the separated fragments correspond to the equilibrium geometry of isolated fragments, only linear configurations have been considered. The zero of energy corresponds to the energy of two singly ionized dimers. The $1/(a+b)$ curve is the Coulomb repulsion term, calculated in assuming that in (a) there is one electronic charge at the center of each dimer, and in (b) that there is one electronic charge at the center of the trimer and one on Mg^+ . Distances are in atomic units and energies in eV.

eling indicates that for the dissociation process of clusters with $n \geq 5$, the increase of energy associated to the breaking of a bond sets in before the longer-range Coulomb repulsion of the holes in the cluster significantly diminishes. Notice also in Fig. 7, that the interatomic distance between the two atoms at the end of the chain is always larger than that of the interior atoms. This is an indication that the end bond is not as strong as the inner bonds, and therefore that for Mg_5^{2+} and Mg_6^{2+} also the barrier height for the evaporative process is lower than for fission. A more detailed analysis of these effects will be published later.

C. Observability and charge localization

We now want to address the problem of the observability of a doubly charged cluster in its metastable minimum. Figure 8 shows that in the case of Mg dimers it is possible to create a doubly charged cluster by a single ionization process. To examine this possibility in the case of trimers, in Fig. 11 we show a representation of the BO surface of Mg_3 , Mg_3^+ and Mg_3^{2+} for the isosceles triangle geometry. This figure shows, that a single-step double

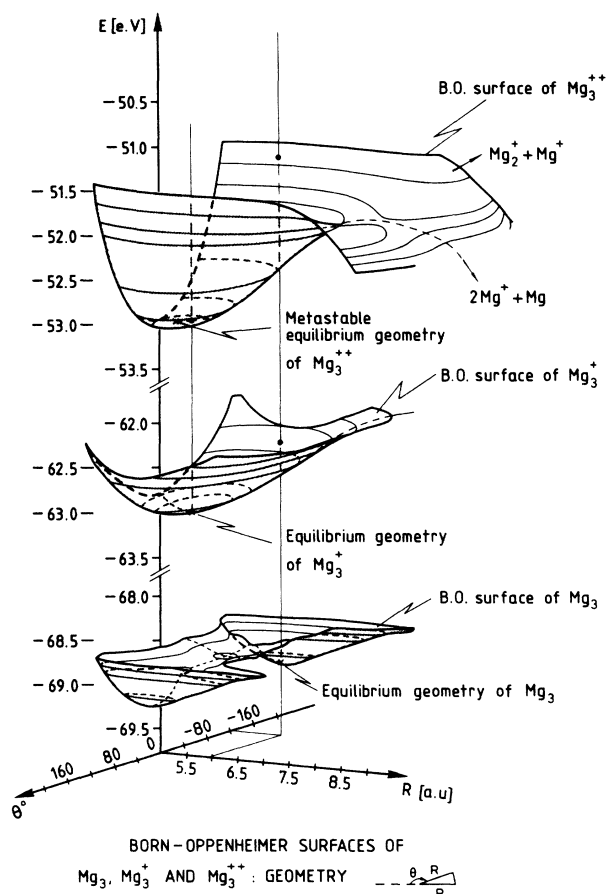


FIG. 11. Born-Oppenheimer surfaces of neutral, singly, and doubly ionized Mg trimers corresponding to various isosceles triangular configurations. E correspond to total energies in the pseudopotential scheme. Distances are in atomic units and energies in eV.

ionization of Mg_3 leads to an equilateral triangle Mg_3^{2+} cluster, whose energy is higher than the dissociation thresholds into $\text{Mg}_2^+ + \text{Mg}^+$ and into $2\text{Mg}^+ + \text{Mg}$. The cluster will then "heat" through the coupling between the electronic and vibronic degrees of freedom, and subsequently fragment. However, a sequential ionization, where one removes a single electron before removing the second electron is also possible, and leads to a metastable doubly charged cluster that is observable. The impossibility of using a single-step ionization process is closely related to the different equilibrium geometries of the neutral (equilateral triangle) and doubly charged (linear-chain) trimers. This situation also occurs for clusters with $n > 3$ and will be discussed in Sec. VII.

In a simple model it has been assumed⁴⁹ that the holes in a doubly charged species are localized and situated on opposite ends of the cluster, as should be true for a linear chain. It is thus interesting to see if that simple picture holds in a more realistic calculation. In order to study this question we have subtracted from the electronic density of a charged cluster, the electronic density of the corresponding neutral cluster with the same geometry. This allows us to study the electron transfer from the neutral to the charged species, and to obtain a view, which is complementary to the standard way of subtracting the electronic density of the atoms, which gives mainly information on the bonding charge. We present such an electronic density difference plot in Fig. 12 for the case of the linear Mg_5^{2+} . The important point is to notice that the holes are mainly localized at the end of the chain, in agreement with the simple picture mentioned before. In the following section we show that the situation is different for a doubly charged triangular bipyramid.

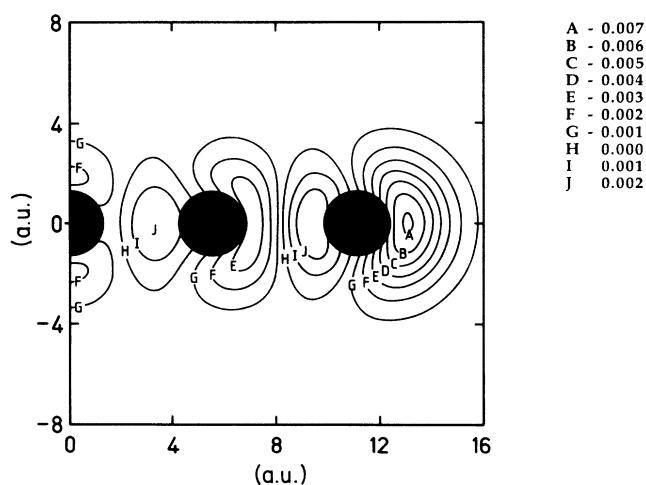


FIG. 12. Contour plot of the difference between the electronic density of linear Mg_5^{2+} at equilibrium distance, and that of a neutral pentamer with the same geometrical structure as Mg_5^{2+} . The length scale is given in atomic units, the electronic density (table on the right-hand side) is given in units of electron per cubic atomic unit. The shaded areas show the extension of the atomic cores.

VII. COMPARATIVE EFFECT OF ELECTRON ATTACHMENT AND DETACHMENT

In this section we focus on a comparative study between the different charged states of a cluster, and especially on the evolution of the geometrical structure as a function of the charge. For this purpose in Fig. 13 we present a summary of the results obtained on the ground state and in several cases the higher-energy configurations of anionic, neutral, cationic, and doubly ionized clusters. The prevalent feature that appears in Fig. 13 is that except for the $n=3$ and $n=4$ cationic clusters the ground-state geometrical structures of the neutral, anionic, and singly ionized clusters are similar, whereas the doubly charged clusters have elongated equilibrium geometries. The changes of structure caused by adding or removing an electron from the neutral cluster are related to Jahn-Teller distortions. In Table VI we give the degeneracy of the Kohn-Sham eigenvalues corresponding to the highest occupied molecular orbital and the lowest unoccupied molecular orbital, as well as the orbital symmetry of the neutral cluster. In the last column, the effect of adding or subtracting an electron on the occurrence of Jahn-Teller distortions is shown.

For $n \leq 6$ the electron which is added to the neutral cluster to form an anionic one, is placed in a molecular orbital that transforms as a one-dimensional representation of the symmetry group of the cluster, and therefore does not lead to a Jahn-Teller distortion. The calculation shows that the anionic clusters keep the group symmetry of the neutral cluster. For $n=7$ the added electron is placed in an orbital that transforms according to a two-dimensional irreducible representation of the symmetry, leading to a Jahn-Teller distortion. However, the cluster is large, and the interatomic distances change by less than 10%. For the smaller cationic trimer and tetramer the Jahn-Teller distortion leads to a dramatic change of structure. For $n=7$, on the other hand, the singly ionized heptamer is large enough that the distortions remain small. This situation is expected to be the rule for clusters larger than $n=7$.

We summarize the points mentioned above in the following way. The neutral clusters have compact geometrical structures. For $n > 4$ the ground-state geometries of the anionic and cationic clusters are obtained from the neutral ones by small displacements of the atoms. They may or may not keep the original symmetry of the neutral cluster depending on the occurrence of the Jahn-Teller distortions.

There is also a tendency to have diminishing interatomic distances from the neutral, to the anion, to the singly and doubly charged cations. This is clear for the dimer case, where the diminishing distance reflects the increasing strength of the bond. This is also apparent for the trimer and tetramer, although there is a discontinuity when the symmetry changes. The situation is, however, more complex for larger clusters, since the interatomic distances of different atoms vary in different ways. In this respect, the pentamer is especially interesting, since it is possible to follow the change of its triangular bipyramidal structure over all charged states, if we take

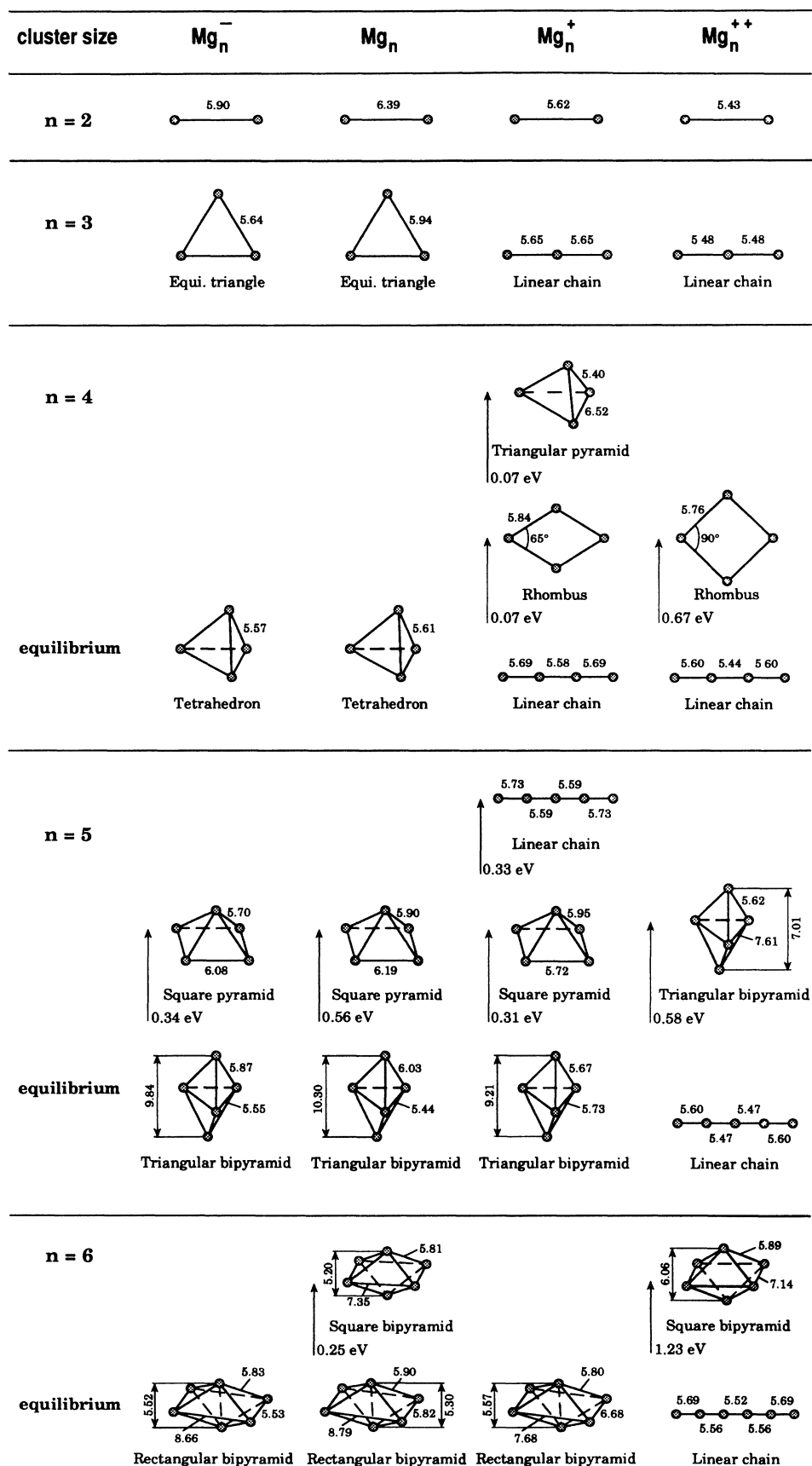


FIG. 13. Lowest-energy geometrical structures of anionic, neutral, singly, and doubly ionized Mg clusters. The difference in energy between different isomers is indicated in the figure. Distances are given in atomic units.

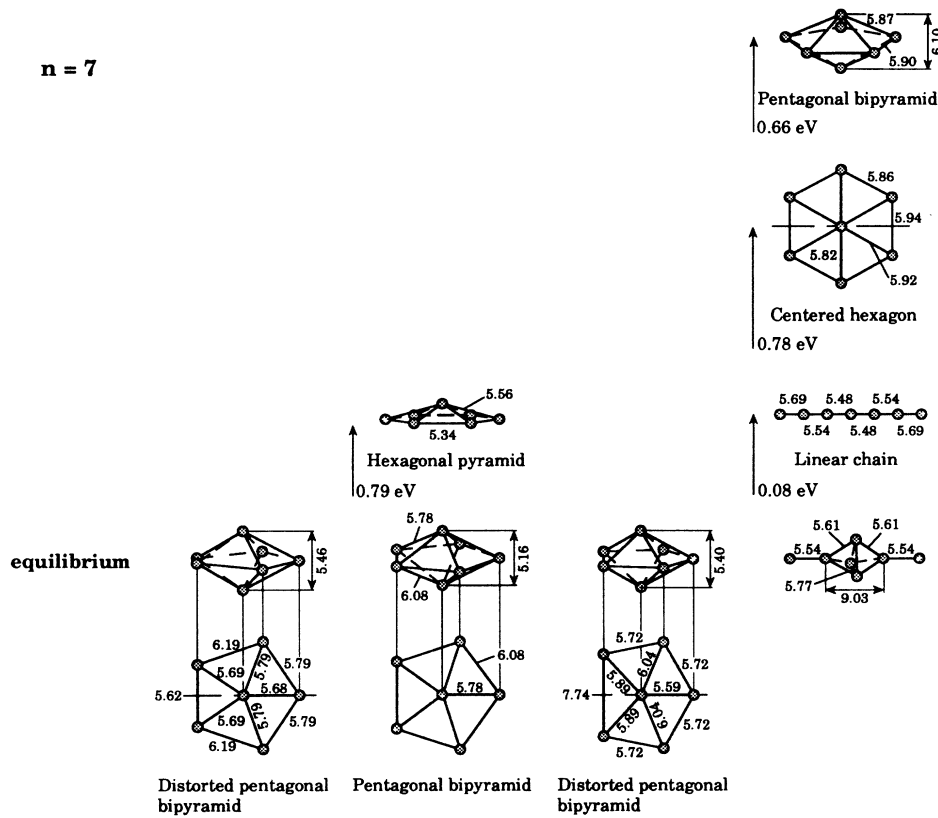


FIG. 13. (Continued).

TABLE VI. Orbital symmetry analysis of Mg_n . Rep. refers to the representation of the symmetry group carried by the orbital eigensubspace. In the last column, the compatibility between the symmetry and the adding or removal of an electron is given.

Mg_3		Geometry: equilateral triangle	Symmetry group: $C_{3v} \times I$	
Eigenvalues	Occupation	Degeneracy	Rep. $C_{3v} \otimes \text{Rep. } I$	Symmetry breaking
-0.095 686	0	1	irreducible	\Rightarrow extra $e^- \Rightarrow$ compatible
-0.161 054	2	2	irreducible	\Rightarrow removed $e^- \Rightarrow$ distortion
Mg_4		Geometry: tetrahedron	Symmetry group: T_d	
Eigenvalues	Occupation	Degeneracy	Rep. T_d	
-0.097 804	0	1	irreducible	\Rightarrow extra $e^- \Rightarrow$ compatible
-0.169 564	3	3	irreducible	\Rightarrow removed $e^- \Rightarrow$ distortion
Mg_5		Geometry: equilateral triangular bipyramid	Symmetry group: $C_{3v} \times I$	
Eigenvalues	Occupation	Degeneracy	Rep. $C_{3v} \otimes \text{Rep. } I$	
-0.098 898	0	1	irreducible	\Rightarrow extra $e^- \Rightarrow$ compatible
-0.142 098	1	1	irreducible	\Rightarrow removed $e^- \Rightarrow$ compatible
Mg_6		Geometry: rectangular bipyramid	Symmetry group: $I_x \times I_y \times I_z$	
Eigenvalues	Occupation	Degeneracy	Rep. $(I_x) \otimes \text{Rep. } (I_y) \otimes \text{Rep. } (I_z)$	
-0.110 440	0	1	irreducible	\Rightarrow extra $e^- \Rightarrow$ compatible
-0.148 226	1	1	irreducible	\Rightarrow removed $\Rightarrow e^-$ compatible
Mg_7		Geometry: pentagonal bipyramid	Symmetry group: $C_{5v} \times I$	
Eigenvalues	Occupation	Degeneracy	Rep. $C_{5v} \otimes \text{Rep. } I$	
-0.108 993	0	2	irreducible	\Rightarrow extra $e^- \Rightarrow$ distortion
-0.153 019	2	2	irreducible	\Rightarrow removed $e^- \Rightarrow$ distortion

into account the doubly ionized isomer, which is only 0.58 eV above the linear ground state. In this case, the interatomic distance in the basal plane increases from the neutral, to the anion, the singly and doubly charged cations, while the height of the bipyramid decreases. There is in particular a large change between the singly and doubly charged clusters, which corresponds to a significant rearrangement of the electronic density.

In order to follow the localization of the electron or hole created in the pentamer, in Fig. 14 we give a two-dimensional contour plot of the total electronic density of the anion, singly, and doubly charged cations, from which the electronic density of a neutral cluster with the same geometry as the corresponding charged cluster has been subtracted. The chosen plane passes through the two summit atoms and one of the basal plane atom. The general features appearing in Fig. 14 are clear. In the case of the anion [Fig. 14(a)] the added electron density is mainly located at the center of the bipyramid and at the exterior of the three base atoms, revealing the bonding character of the center part electron density. For the singly charged cation [Fig. 14(b)] the hole density is predominantly located at the exterior of the summit atoms. For the doubly charged cluster [Fig. 14(c)] the largest hole density is situated at the exterior of the three basal plane atoms, a sizable hole density is also placed near the two summit atoms. There is thus an important modification of the hole density from the singly to the doubly charged cation. This modification is reflected in the geometry: the interatomic distance in the basal plane increases substantially, in order to keep the holes as far apart as possible, while keeping a strong bonding between the summit and the basal plane atoms.

A detailed analysis of the hole density has not been done for all doubly charged clusters, but the picture that emerges seems clear. In the case of the linear chains, the holes are mainly situated at the extremities of the chain in order to minimize their Coulomb repulsion. In the case of three-dimensional structures, the holes locate at the exterior of all atoms and the structure deforms in order to keep the holes as far apart as possible, while maintaining short interatomic distances for other atoms. The $n = 6$ case is consistent with this picture. The rectangular basal plane of the hexamer deforms from an elongated rectangle for the neutral cluster toward a square bipyramid isomer for the doubly charged cluster, where the interatomic distance in the basal plane is large.

We mentioned in Sec. VI for trimers that the differing geometries of the neutral and cationic clusters imposes constraints on the observability of doubly charged clusters. This situation is more general and usually occurs when the geometries of the neutral and charged species are different. Looking at Fig. 13 and the case $n = 4$, it is clear that the single-ionization process from the tetrahedron toward the linear chain is not favored. It is more probable that, after vertical ionization, the structure will relax toward the triangular pyramid isomer, which is only 0.17 eV lower in energy than the energy of the tetrahedra derived from vertical ionization of the neutral cluster. In the $n = 5$ case it is also probable for the same reasons that, by ionizing the triangular bipyramid cation,

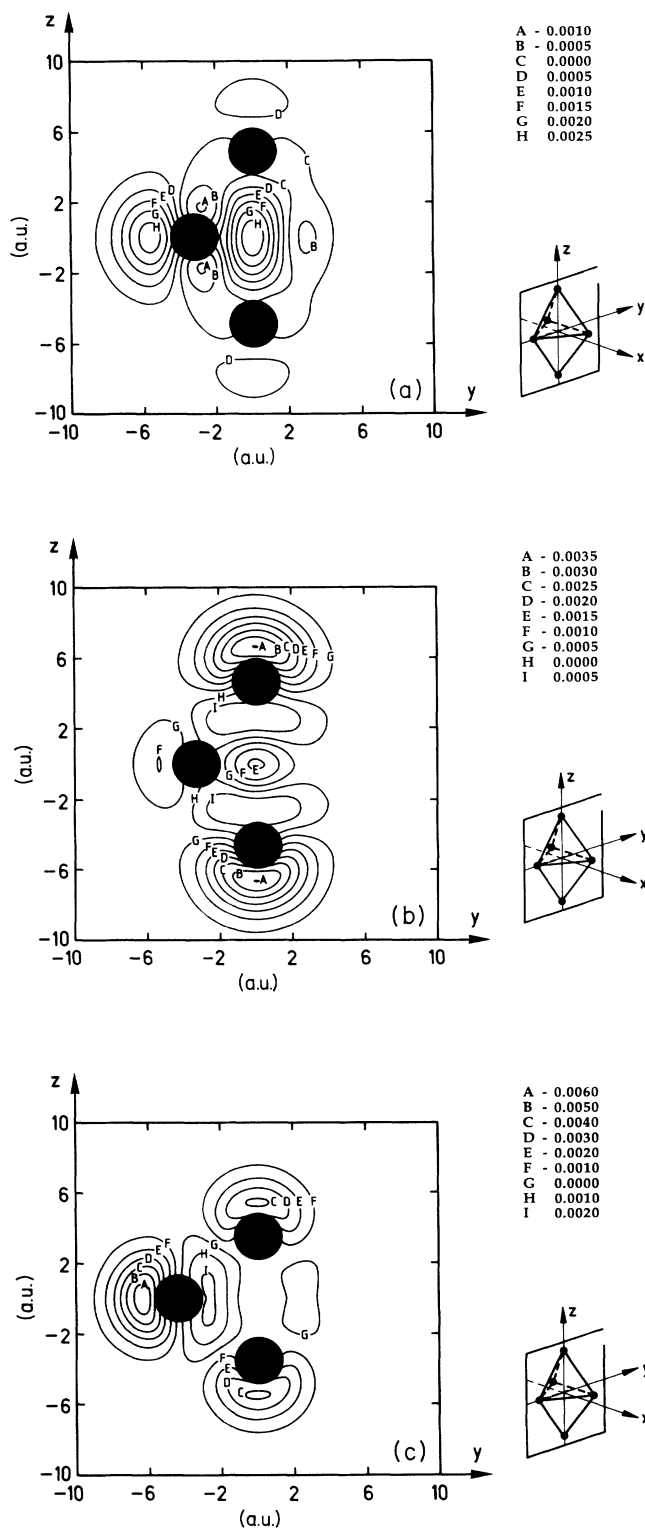


FIG. 14. Contour plots of the difference between the electronic density of a charged triangular bipyramid cluster, and that of a neutral cluster with the same geometrical structure as the charged cluster; (a) is for the anion, (b) for the singly charged cation, and (c) for the doubly charged cation. The chosen plane is indicated in the figure. The length scale is given in atomic units, the electronic density (table on the right-hand side) is given in units of electron per cubic atomic unit. The shaded areas show the extension of the atomic cores.

TABLE VII. Electron affinity (EA) ionization potential of neutral (IP1) and of singly charged cationic clusters (IP2). Both the vertical and adiabatic values are given (eV).

n	EA		IP1		IP2	
	Adiab.	Vert.	Adiab.	Vert.	Adiab.	Vert.
1			7.63	7.63	15.05	15.05
2	0.38	0.39	6.32	6.42	11.68	11.70
3	0.90	0.93	5.85	6.43	9.92	9.93
4	0.99	1.00	6.28	6.61	8.82	8.82
5	1.09	1.14	5.50	5.71	8.67	9.68
6	1.40	1.46	5.71	5.76	7.84	9.25
7	1.46	1.52	5.57	5.87	8.02	9.13
bulk	3.64		3.64		3.64	

one ends up with the doubly charged triangular bipyramid isomer, which is 0.4 eV lower in energy than the bipyramid obtained by vertical ionization. The same is also true for the $n = 6$ and $n = 7$ clusters.

These examples show that, for reasons related to the geometrical structures of the neutral and charged species, the ionization process may favor isomers, rather than the true ground-state geometrical structure.

We conclude this section by presenting the results for the adiabatic and vertical ionization potentials (IP's) and electron affinities, which are summarized in Table VII. Notice that for $n = 5, 6,$ and 7 the differences between the adiabatic and vertical values of the second ionization potential are significantly different, due to the different geometries of the singly and doubly ionized species. We represent the adiabatic and vertical values in Fig. 15 as a function of $N^{-1/3}$, since the classical drop model gives a straight line in this representation. We have also reported the results of a more realistic approximation,⁵⁰ which takes into account the spill out of the electrons beyond the classical radius R . Our theoretical values for both the first ionization potential and the electron affinity are well

approximated by the simple liquid-drop model. This is in agreement with the observations made for several non-transition metals,⁵¹ but does not agree with the measurements reported for mercury clusters.¹⁷ In this case the atomic ionization potential is about 2 eV above the $1/r$ curve, and the measured IP's remain so up to $n \sim 13$, after which they gradually converge toward the drop model behavior. This was given as an indication of the van der Waals to metallic transition in mercury clusters. Such a measure will not give similar information in the case of Mg, since the atomic value is already well fitted by the simple liquid drop model.

VIII. CONCLUSIONS

We have carried out pseudopotential local-spin-density calculations on neutral, anionic, cationic, and doubly ionized Mg clusters ($n \leq 7$). Our results show that the nature of the bond changes as the size increases. If the s - p hybridization is taken as a criteria of metallic behavior, our analysis shows that Mg₇ is not metallic. However, all atoms of the clusters that we have studied are surface atoms, and the qualitative behavior may change when "bulk" atoms appear for larger clusters. We also expect that the symmetry plays an important role in the convergence toward metallic behavior. Once the metallic behavior is established, a nonjellium-to-jellium transition, similar to that observed for Al clusters,⁵² may also occur.

Whereas a single Mg atom has no electron affinity, our studies show that Mg _{n} clusters ($n \geq 2$) have electron affinities, which increase with increasing cluster size. The calculated values are in excellent agreement with recent data obtained by photoelectron detachment spectroscopy. The extra electron occupies a bonding orbital with dominant p character, which enhances the stability of the neutral cluster. Its symmetry explains why the anionic clusters have geometries similar to the neutral clusters. Small cationic clusters ($n = 3,$ and 4) have linear chain geometries, however, the larger cluster's geometries can be derived from the neutral ground-state configuration through small displacements of the atoms.

Our studies on doubly ionized clusters show that their geometries are dictated by the Coulomb repulsion between the holes and the electronic bonding forces. At small sizes the Coulomb forces dominate and the struc-

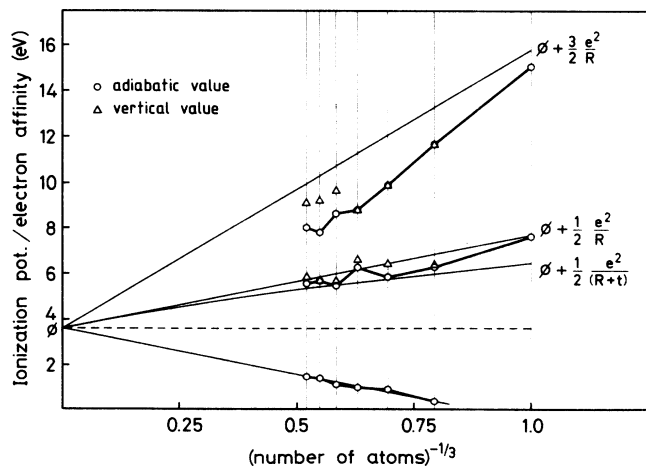


FIG. 15. Ionization potential and electron affinity of Mg clusters as a function of $n^{-1/3}$. The $\Phi + e^2/2R$ and $\Phi + 3e^2/2R$ curves are the prediction of the simple liquid-drop model, the $\Phi + \frac{1}{2}e^2/(R+t)$ curve takes into account the spill out of the electronic density with $t = 1.4$ a.u. R is the classical radius equal to $n^{1/3}r_s$.

tures are linear chains. Mg_7^{2+} is the smallest doubly ionized cluster, where the geometry reflects the competition between the bonding and the repulsive forces. The clusters that we have calculated are metastable, they are protected from fragmentation by barriers of ~ 1 eV, and so it should be possible to observe them. The dissociation energy of Mg_7^{2+} is only -0.27 eV, compared to -2.54 eV for Mg_2^{2+} , we expect clusters with $n \sim 10$ to be energetically stable.

We also give results on the dissociation behavior of doubly charged clusters ($n > 3$) and a complete study of the BO surfaces of neutral and ionized trimers. These studies indicate that the ionization process will select isomers, rather than the true ground-state geometry, depending on geometry constraints. However, a more detailed analysis of these effects has still to be done.

Note added in proof. In a recent paper G. Durand [J.

Chem. Phys. **91**, 6225 (1989)] has calculated the structure and stability of Mg_n^+ and Mg_n^{2+} clusters, using a model Hamiltonian ($n \leq 7$) and CI method ($n \leq 4$). Our results are in reasonable agreement with the CI calculations.

ACKNOWLEDGMENTS

We thank C. Nussbaum, who developed for us the computer program for the graphical presentation and the analysis of our results. We also thank W. de Heer for a critical reading of the manuscript and very helpful suggestions. We acknowledge support from the Swiss National Fund (Contract No. 20-26535.89 and No. 29-544687) and one of us (S.N.K.) acknowledges support from the U.S. Department of energy (Grant No. DE-FG05-87ER45316).

*Permanent address: Commonwealth University, Richmond, Virginia 23284.

†Permanent address: Institut Romand de Recherche Numérique en Physique des Matériaux, Ecole Polytechnique Fédérale de Lausanne, PHB-Ecublens, CH-1015 Lausanne, Switzerland.

¹L. A. Bloomfield, R. R. Freeman, and W. L. Brown, Phys. Rev. Lett. **54**, 2246 (1985).

²W. A. Saunders, P. Fayet, and L. Wöste, Phys. Rev. A **39**, 4400 (1989).

³C. Bréchnignac, Ph. Cahuzac, J. Leygnier, R. Pflaum, and J. Weiner, Phys. Rev. Lett. **61**, 314 (1988); W. A. Saunders, *ibid.* **62**, 1037 (1989).

⁴D. G. Leopold, J. Ho, and W. C. Lineberger, J. Chem. Phys. **86**, 1715 (1987).

⁵O. Echt, in *Physics and Chemistry of Small Clusters*, edited by P. Jena, B. K. Rao, and S. N. Khanna (Plenum, New York, 1987).

⁶J. Koutecky and P. Fantucci, Chem. Rev. **86**, 539 (1986).

⁷J. L. Martins, J. Buttet, and R. Car, Phys. Rev. B **31**, 1804 (1985).

⁸I. Boustani, W. Pewestorf, P. Fantucci, V. Bonacic-Koutecky, and J. Koutecky, Phys. Rev. B **35**, 9437 (1987); V. Bonacic-Koutecky, P. Fantucci, and J. Koutecky, *ibid.* **37**, 4369 (1988).

⁹I. Boustani and J. Koutecky, J. Chem. Phys. **88**, 5657 (1988).

¹⁰C. W. Bauschlicher, Jr., S. R. Langhoff, and P. R. Taylor, J. Chem. Phys. **88**, 1041 (1988).

¹¹J. Flad, G. Igel-Mann, H. Preuss, and H. Stoll, Chem. Phys. **90**, 257 (1984).

¹²K. Raghavachari and V. Logovinsky, Phys. Rev. Lett. **55**, 2853 (1985).

¹³F. Reuse, S. N. Khanna, V. de Coulon, and J. Buttet, Phys. Rev. B **39**, 12911 (1989).

¹⁴S. N. Khanna, F. Reuse, and J. Buttet, Phys. Rev. Lett. **61**, 535 (1988).

¹⁵W. A. de Heer, W. D. Knight, M. Y. Chou, and M. L. Cohen, in *Solid State Physics*, edited by F. Steitz and D. Turnbull (Academic, New York, 1987), Vol. 40.

¹⁶R. O. Jones, J. Chem. Phys. **71**, 1300 (1979).

¹⁷K. Rademann, Ber. Bunsenges. Phys. Chem. **93**, 653 (1989); K. Rademann, B. Kaiser, U. Even, and F. Hensel, Phys. Rev. Lett. **59**, 2319 (1987); C. Bréchnignac, M. Broyer, Ph. Cahuzac,

G. Delacrétaz, P. Labastie, J. P. Wolf, and L. Wöste, *ibid.* **60**, 275 (1988).

¹⁸G. M. Pastor, P. Stampfli, and K. H. Bennemann, Phys. Scr. **38**, 623 (1988); G. M. Pastor, P. Stampfli, and K. H. Bennemann, Europhys. Lett. **7**, 419 (1988).

¹⁹P. Ballone and G. Galli, Phys. Rev. B **40**, 8563 (1989).

²⁰R. P. Neisler and K. S. Pitzer, J. Phys. Chem. **91**, 1084 (1987).

²¹C. W. Bauschlicher, Jr., and L. G. M. Pettersson, J. Chem. Phys. **84**, 2226 (1986); M. M. Marino and W. C. Ermler, *ibid.* **86**, 6283 (1987).

²²C. W. Bauschlicher, Jr., P. S. Bagus, and B. N. Cox, J. Chem. Phys. **77**, 4032 (1982); G. Pacchioni and J. Koutecky, *ibid.* **77**, 5850 (1982); P. S. Bagus, C. J. Nelin, and C. W. Bauschlicher, Surf. Sci. **156**, 615 (1985); R. A. Chiles and C. E. Dykstra, J. Chem. Phys. **75**, 1044 (1981).

²³G. Durand, J.-P. Daudey, and J.-P. Malrieu, J. Phys. **47**, 1335 (1986).

²⁴W. Schulze, B. Winter, and I. Goldenfeld, Phys. Rev. B **38**, 12937 (1988).

²⁵C. Bréchnignac, M. Broyer, Ph. Cahuzac, G. Delacrétaz, P. Labastie, and L. Wöste, Chem. Phys. Lett. **133**, 45 (1987).

²⁶F. Liu, M. R. Press, S. N. Khanna, and P. Jena, Phys. Rev. Lett. **59**, 2562 (1987).

²⁷G. B. Bachelet, D. R. Hamann, and M. Schlüter, Phys. Rev. B **26**, 4199 (1982).

²⁸D. M. Ceperley and B. J. Alder, Phys. Rev. Lett. **45**, 566 (1980); J. P. Perdew and A. Zunger, Phys. Rev. B **23**, 5048 (1981).

²⁹*Molecular Spectra and Molecular Structure*, edited by K. P. Huber and G. Herzberg (Van Nostrand/Reinhold, New York, 1979).

³⁰R. O. Jones, in *Ab Initio Methods in Quantum Chemistry—I*, edited by K. P. Lawley (Wiley, New York, 1987).

³¹P. Hohenberg and W. Kohn, Phys. Rev. **136**, B864 (1964); W. Kohn and L. J. Sham, *ibid.* **140**, A1133 (1965).

³²F. Reuse and M. Bessat, Diplomarbeit, Ecole Polytechnique Fédérale de Lausanne, 1988.

³³T. H. Upton, J. Chem. Phys. **86**, 7054 (1987); T. H. Upton, Phys. Rev. Lett. **56**, 2168 (1986).

³⁴G. Chalasinski, D. J. Funk, J. Simons, and W. H. Breckenridge, J. Chem. Phys. **87**, 3569 (1987).

³⁵A. R. Williams and U. von Barth, in *Theory of the Inhomogeneous Electron Gas*, edited by S. Lundqvist and N. H.

- March (Plenum, New York, 1983), Chap. 4.
- ³⁶M. Y. Chou, P. K. Lam, and M. L. Cohen, *Phys. Rev. B* **28**, 4179 (1983).
- ³⁷C. W. Bauschlicher, Jr., and H. Partridge, *J. Chem. Phys.* **80**, 334 (1984).
- ³⁸R. Linke, J. L. Morán-López, and K. H. Bennemann, *Phys. Rev. B* **27**, 7348 (1983); L. F. Mattheiss and W. W. Warren, Jr., *ibid.* **16**, 624 (1977).
- ³⁹K. Rademann, *Ber. Bunsenges. Phys. Chem.* **93**, 653 (1989), and (private communication).
- ⁴⁰R. P. Gubta and A. J. Freeman, *Phys. Rev. Lett.* **36**, 1194 (1976).
- ⁴¹J. P. Perdew and A. Zunger, *Phys. Rev. B* **23**, 5048 (1981).
- ⁴²H. B. Shore, J. H. Rose, and E. Zaremba, *Phys. Rev. B* **15**, 2858 (1977).
- ⁴³S. Mukherjee, F. Reuse, S. N. Khanna, and J. Buttet (unpublished).
- ⁴⁴K. D. Jordan and J. Simons, *J. Chem. Phys.* **77**, 5250 (1982).
- ⁴⁵K. D. Jordan and J. Simons, *J. Chem. Phys.* **67**, 4027 (1977); K. D. Jordan and J. Simons, *ibid.* **72**, 2889 (1980).
- ⁴⁶Y. Liu, Q.-L. Zang, F. K. Tittel, R. F. Curl, and R. E. Smalley, *J. Chem. Phys.* **85**, 7434 (1986).
- ⁴⁷G. Gantefor and K. H. Meiwes-Broer (private communication).
- ⁴⁸O. Gunnarson and B. I. Lundqvist, *Phys. Rev. B* **13**, 4274 (1976).
- ⁴⁹D. Tomanek, S. Mukherjee, and K. H. Bennemann, *Phys. Rev. B* **28**, 665 (1983).
- ⁵⁰J. P. Perdew, *Phys. Rev. B* **37**, 6175 (1988).
- ⁵¹M. D. Morse, *Chem. Rev.* **86**, 1049 (1986).
- ⁵²W. A. de Heer, P. Milani, and A. Châtelain, *Phys. Rev. Lett.* **63**, 2834 (1989).

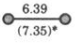
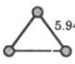
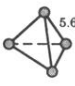
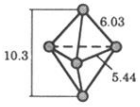
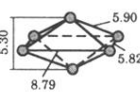
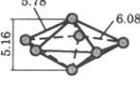
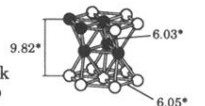
Cluster size	Equilibrium geometry (a.u.)	Atomization energies (eV)			Valence electrons Mulliken popul. e^-	
		AE	AE/atom	AE/bond	s	p
2		0.22	0.11	0.22	0.94	0.06
3		0.78	0.26	0.26	0.87	0.13
4		2.00	0.50	0.33	0.80	0.20
5		2.50	0.50	0.28	0.83	0.17
6		3.15	0.53	0.29	0.83	0.17
7		4.23	0.60	0.26	0.81	0.19
bulk hcp		1.52*	0.25*	0.39*	0.56*	

FIG. 1. Equilibrium geometry, atomization energy (AE), and valence electron Mulliken population of neutral Mg clusters. Distances are given in atomic units and energies in eV. The numbers marked with an asterisk are the known experimental values. The bulk Mulliken population is taken from Ref. 40.

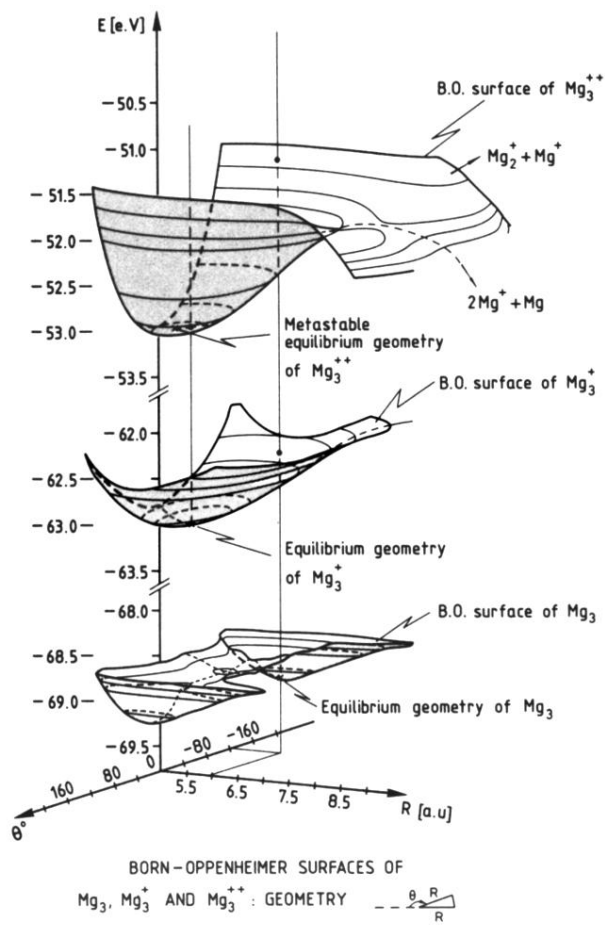


FIG. 11. Born-Oppenheimer surfaces of neutral, singly, and doubly ionized Mg trimers corresponding to various isosceles triangular configurations. E correspond to total energies in the pseudopotential scheme. Distances are in atomic units and energies in eV.

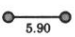

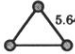
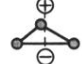

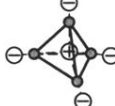
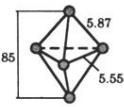
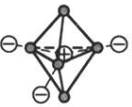
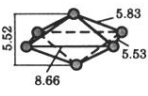
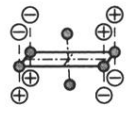
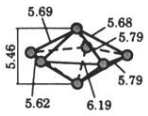
Cluster size	Equilibrium geometry (a.u.)	AE/atom	Symmetry extra orbital	Extra electron Mulliken popul.	
				s	p
2		0.29		0.00	1.00
3		0.57		0.00	1.00
4		0.74		0.36	0.64
5		0.74		0.37	0.63
6		0.76		0.00	1.00
7		0.81		0.00	1.00

FIG. 4. Equilibrium geometry, atomization energy per atom (AE/atom), symmetry of the extra electron orbital, and extra orbital Mulliken population analysis of singly negatively charged Mg clusters. The atomization energy is defined as the difference between the energy of n separated atoms and the energy of Mg_n^- . Distances are given in atomic units and energies in eV.

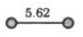
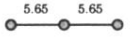

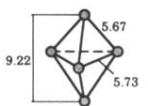
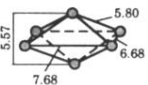
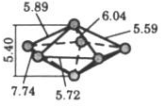
Cluster size	Equilibrium geometry (a.u.)	Atomization energies (eV)	
		AE	AE/atom
2		1.52	0.76
3		2.54	0.85
4		3.33	0.83
5		4.63	0.93
6		5.05	0.84
7		6.30	0.90

FIG. 6. Equilibrium geometry and atomization energy (AE) of singly ionized clusters. The atomization energy is defined as $(n - 1) E + E^+ - E_n^+$, where E and E^+ are the energies of, respectively, neutral and singly ionized atoms. Distances are given in atomic units, and energies in eV.

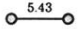
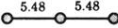
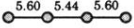
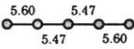
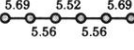
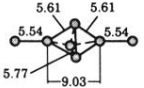
Cluster size	Atomization energies (eV)	Equilibrium geometry	Dissoc. channel	Dissoc. energy (eV)	Barrier (eV)
2	-1.27		$Mg^+ + Mg^+$ $Mg^{2+} + Mg$	-2.54 4.88	0.48
3	0.07		$Mg_2^+ + Mg^+$ $Mg^+ + Mg^+ + Mg$	-1.30 0.22	0.77
4	0.53		$Mg_2^+ + Mg_2^+$ $Mg_3^+ + Mg^+$ $Mg_2^+ + Mg^+ + Mg$	-0.92 -0.41 0.61	0.90 0.82
5	0.72		$Mg_3^+ + Mg_2^+$ $Mg_4^+ + Mg^+$	-0.48 0.25	0.98
6	0.80		$Mg_3^+ + Mg_3^+$ $Mg_4^+ + Mg_2^+$ $Mg_5^+ + Mg^+$	-0.29 -0.05 0.15	1.03 1.03
7	0.84		$Mg_5^+ + Mg_2^+$ $Mg_4^+ + Mg_3^+$	-0.27 0.02	

FIG. 7. Equilibrium geometry, atomization energy, and dissociation channels of doubly ionized clusters. The atomization energy is defined as $(n-2)E + 2E^+ - E_n^{2+}$. The dissociation energy measures the difference in energy between the fragments and the parent cluster, a minus sign indicates that Mg_n^{2+} is metastable with respect to the corresponding fragments. The barrier height has been calculated in assuming that the interatomic distances of the separated fragments correspond to the equilibrium geometry of isolated fragments. Only linear configurations have been considered. Distances are given in atomic units, and energies in eV.